Rapid Communications | Editors' Suggestion

Weak localization measurements of electronic scattering rates in Li-doped epitaxial graphene

A. Khademi,[1,2,*] K. Kaasbjerg,[3] P. Dosanjh,[1,2] A. Stöhr,[4] S. Forti,[4,†] U. Starke,[4] and J. A. Folk[1,2,‡]

[1]*Stewart Blusson Quantum Matter Institute, University of British Columbia, Vancouver, BC, Canada V6T1Z4*

[2]*Department of Physics and Astronomy, University of British Columbia, Vancouver, BC, Canada V6T1Z1*

[3]*Center for Nanostructured Graphene (CNG), Department of Physics, Technical University of Denmark, DK-2800 Kongens Lyngby, Denmark*

[4]*Max Planck Institute for Solid State Research, 70569 Stuttgart, Germany*

(Received 31 August 2019; revised manuscript received 16 October 2019; published 29 October 2019)

Early experiments on alkali-doped graphene demonstrated that the dopant adatoms modify the conductivity of graphene significantly, as extra carriers enhance conductivity while Coulomb scattering off the adatoms suppresses it. However, conductivity probes the overall scattering rate, so a dominant channel associated with long-range Coulomb scattering will mask weaker short-range channels. We present weak localization measurements of epitaxial graphene with lithium adatoms that separately quantify intra- and intervalley scattering rates, then compare the measurements to tight-binding calculations of expected rates for this system. The intravalley rate is strongly enhanced by Li deposition, consistent with Coulomb scattering off the Li adatoms. A simultaneous enhancement of intervalley scattering is partially explained by extra carriers in the graphene interacting with residual disorder. But differences between measured and calculated rates at high Li coverage may indicate adatom-induced modifications to the band structure that go beyond the applied model. Similar adatom-induced modifications of the graphene bands have recently been observed in angle-resolved photoemission spectroscopy, but a full theoretical understanding of these effects is still in development.

DOI: 10.1103/PhysRevB.100.161405

Adatoms have frequently been proposed as a way to alter the electronic properties of graphene: to make it superconducting [1–4], magnetic [5,6], or even a topological insulator [7,8]. Despite the conceptual simplicity of depositing selected elements onto the exposed surface of a graphene sheet, many of the more exotic predictions for novel adatom-induced electronic states in graphene have proven difficult to realize in experiment. In order to push this area forward, experimental feedback is needed to clarify the impact of adatoms on the electronic properties of graphene.

The interaction of alkali adatoms with graphene is expected to be particularly simple, and represents a logical starting point to address the graphene-adatom puzzle. Alkali-metal atoms are known to be efficient dopants, transferring around one electron each to the graphene lattice [9–11] while the positively charged ions that remain cause strong Coulomb scattering [9,12,13]. The graphene-lithium system is especially interesting due to a recent report of superconductivity with a critical temperature near 6 K [14]. More generally, a variety of recent results indicate that adatoms must be thought of as fundamentally modifying the graphene band structure rather than than simply as perturbations on the conventional Dirac structure [14–17].

Here, we present magnetoresistance measurements of weak localization (WL) in Li-doped graphene that probe the interaction between graphene's conduction electrons and the Li adatoms. The analysis of WL data offers detailed information about intra- and intervalley scattering channels, which are depicted schematically in Fig. 1(a). In addition to the expected enhancement of intravalley scattering, our data indicate that intervalley scattering between graphene's K and K' valleys is strongly enhanced at high Li coverage. The increase of intervalley rate due to alkali-metal adatoms is reminiscent of a previous report in Li-intercalated bilayer graphene [18].

At first glance these results are surprising, because scattering off Li is expected to be long range in character, and therefore not capable of inducing the large momentum shifts required for intervalley scattering [Fig. 1(a)]. In this way, lithium contrasts with other adatoms and substitutionals that are expected to introduce both Coulomb and short-range scattering in graphene [19–21]. Our data can partially be accounted for through enhanced scattering off preexisting short-range disorder, as confirmed by a tight-binding analysis of scattering rates and conductivity that includes trigonal warping and the nonlinearity in the band structure away from the Dirac point. But a discrepancy remains between experimental data and tight-binding predictions for the intervalley rate at high Li coverage, pointing to adatom-induced band-structure modifications that go beyond our modeling. Such modifications would be consistent with angle-resolved photoemission spectroscoppy (ARPES) experiments [14–16] and recent theoretical calculations [17].

Measurements are reported on four epitaxial monolayer graphene samples: SiC1 was grown on a weakly doped 6H-SiC(0001) surface [22]; SiC2–4 were cut from commercially

*Present address: Department of Electrical and Computer Engineering, University of Victoria, Victoria, British Columbia, Canada V8P 5C2.

†Present address: Centre for Nanotechnology Innovation IIT@NEST, Piazza San Silvestro 12, 56127 Pisa, Italy.

‡jfolk@physics.ubc.ca

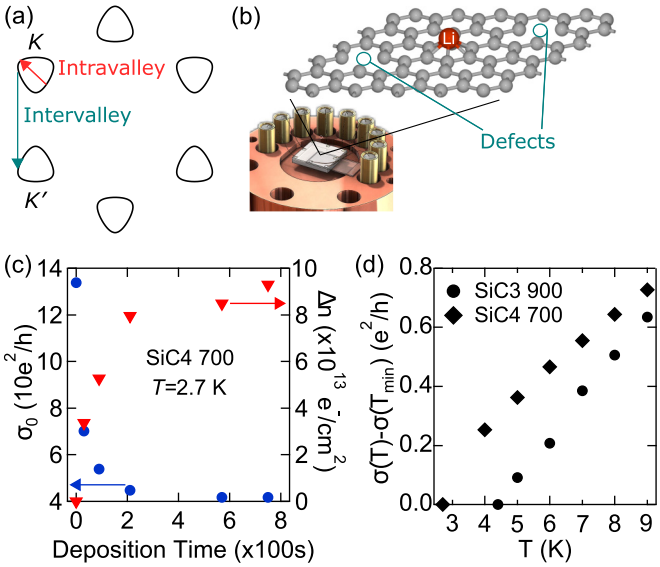

FIG. 1. (a) Intra- and intervalley scattering processes illustrated in a constant energy contour. (b) Annealing stage, showing the SiC chip glued to the end of a quartz plate. Illustration of graphene lattice on the chip, with vacancies that would cause intervalley scattering as well as a Li adatom. (c) Decrease in conductivity due to consecutive Li depositions. Right axis: Li-induced carrier density $\Delta n \equiv n - n_0$, starting from initial density $n_0 = 2.18 \times 10^{13}$ cm^{-2}. (d) Conductivity of graphene samples decreases monotonically with temperature down to the lowest temperatures ($T_{\min}$) accessed in our measurements, even after depositing Li to the point where the carrier density saturated. This panel shows the temperature-dependent conductivity change compared to the conductivities at $T_{\min}$: $\sigma(T_{\min} = 2.7\ \text{K}) = 41.8e^2/h$ for SiC4 700 and $\sigma(T_{\min} = 4.4\ \text{K}) = 35.1e^2/h$ for SiC3 900.

available epitaxial graphene grown on the semi-insulating 4H-SiC(0001) surface [23]. The labeling of SiC1–4 is consistent with an earlier doping study on these samples [24], where further sample details can be found. After growth, eight contacts were deposited by thermal evaporation onto the corners and edges of each sample, using shadow evaporation to avoid polymer resist contamination. Resistances were measured in a four-probe quasi–van der Pauw configuration, then converted to conductivities for comparison with weak localization theory.

Experiments were performed in a UHV chamber with base pressure below 5×10^{-10} torr, with Li evaporated from an SAES getter source while the sample was held at 4 K on a liquid-He cooled cold finger. A custom stage [Fig. 1(b)] enabled annealing operations up to 900 K while also ensuring cryogenic thermal contact between the sample and the cold finger during transport measurements [24]. The stage could be cooled below 3 K by pumping on the liquid He line. Photographs of several samples on this stage can be seen in Supplemental Material Fig. S1 [25].

The first step in each experiment was a three-day bakeout of both sample and chamber at 390 K. For some samples, further annealing of the chip was performed using the stage [Fig. 1(b)] [24]. Then, the sample and a surrounding shroud were cooled down to 3–4 K, and Li was deposited in multiple increments. The shroud was open only during Li depositions, then closed again before magnetoresistance measurements were performed. Carrier density was determined by transverse magnetoresistance (the classical Hall effect) after each deposition, while the scattering rates that are central to this Rapid Communication were determined from the longitudinal magnetoresistance through WL.

It has previously been shown that high temperature annealing prior to Li deposition is crucial to achieving efficient graphene-Li coupling [24]. Here, we explore samples with a range of preparations: SiC1 and SiC2 were measured with no higher temperature anneals following the 390 K bakeout. SiC3 underwent one Li deposition-and-measurement sequence right after bakeout, then it was annealed at 900 K (which desorbed the Li) and a second Li deposition-measurement sequence was performed. SiC4 was annealed first at 500 K, then a Li deposition-measurement sequence was performed, then it was annealed again at 700 K before a second deposition-measurement sequence. For clarity, data from a given sequence is labeled by the sample name and the most recent annealing temperature in Kelvin. For example, SiC1 390 refers to sample SiC1 with no additional anneal after the 390 K bakeout.

Figure 1(c) illustrates an example of doping level and conductivity changes resulting from consecutive Li depositions. For SiC4 700, the induced carrier density due to Li saturated around $10^{14}e^-/\text{cm}^2$ while the conductivity decreased by a factor of 4. For SiC3 900, annealed at a higher temperature, the saturation carrier density was a factor of 2 larger [Fig. S2(a) [25]]. The saturation of carrier density in our samples, with increasing Li deposition, was discussed in Ref. [24], and presumably results from insufficient surface preparation.

All samples showed a weakly insulating temperature dependence of conductivity below around 10 K. Figure 1(d) shows this behavior for SiC3 900 and SiC4 700 after their final Li depositions (see Supplemental Material Fig. S2(b) for SiC3 390 and SiC4 500 [25]). The observed conductivities were consistent in all cases with the logarithmic dependence expected for weak localization and the electron-electron correction to conductivity in 2D. The fact that the conductivity changed smoothly with the cold finger temperature down to 2.7 K confirms the efficient thermal coupling of our sample stage design. No upturn in conductivity at low temperature was observed in any samples, as might have been expected if superconductivity ($T_c \sim 6$ K) were induced in these samples by the Li [14].

The expected WL dip in longitudinal conductivity at zero magnetic field [Fig. 2(a)] was observed in all samples. Electronic scattering rates were extracted by fitting to the standard WL form for graphene [26]:

$$\Delta\sigma(B_\perp) = \sigma(B_\perp) - \sigma(0) = \frac{e^2}{\pi h}\left[F\left(\frac{\tau_B^{-1}}{\tau_\varphi^{-1}}\right) - F\left(\frac{\tau_B^{-1}}{\tau_\varphi^{-1} + 2\tau_i^{-1}}\right) - 2F\left(\frac{\tau_B^{-1}}{\tau_\varphi^{-1} + \tau_*^{-1} + \tau_i^{-1}}\right)\right], \quad (1)$$

where $F(z) = \ln(z) + \psi(\frac{1}{z} + \frac{1}{2})$, ψ is the digamma function, and $\tau_B^{-1} = 4eDB_\perp/\hbar$ is the phase accumulation rate in magnetic field $B_\perp$ with diffusion constant D. τ_φ^{-1} represents the

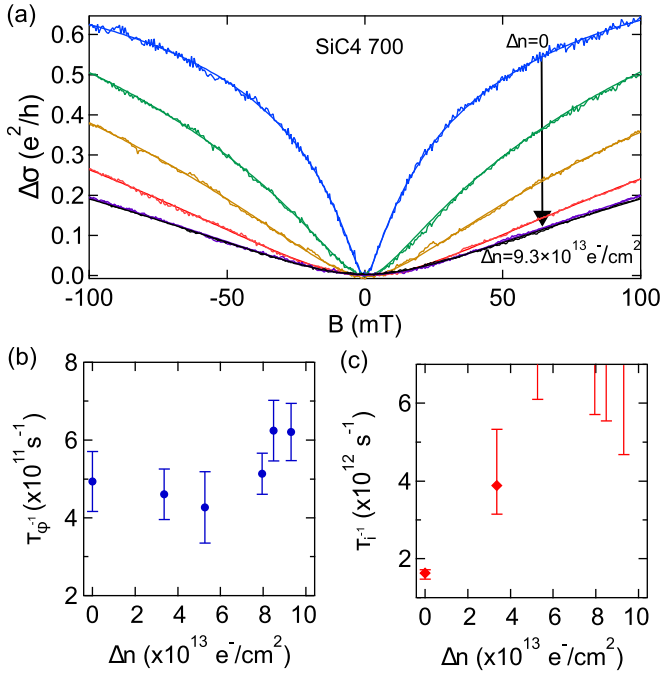

FIG. 2. (a) The effect of Li deposition on magnetoconductivity, $\Delta\sigma \equiv \sigma(B) - \sigma(B = 0)$. As in Fig. 1, Δn represents increase carrier density due to Li, starting from $n_0 = 2.18 \times 10^{13}$ cm^2. The solid lines are fits to Eq. (1). Extracted dephasing (b) and intervalley (c) rate versus induced carrier density due to Li. All data correspond to SiC4 700 at $T = 2.7$ K.

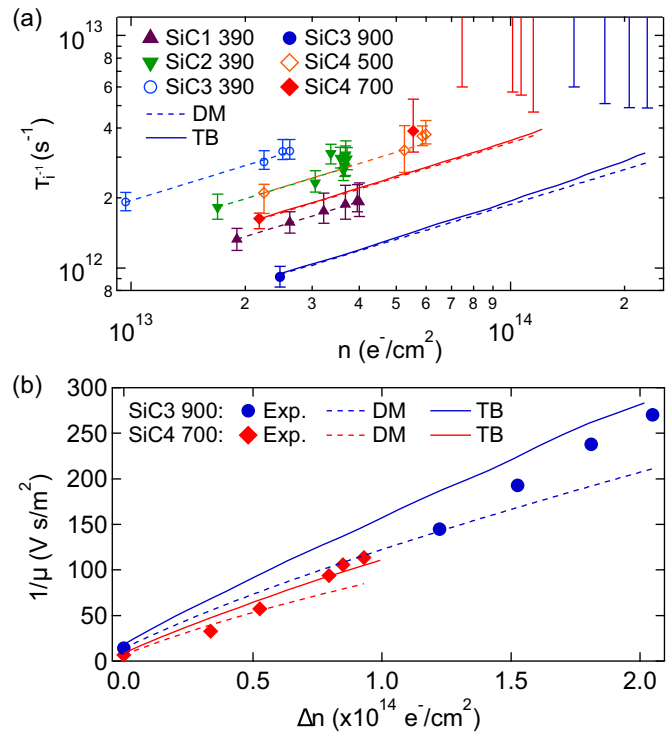

FIG. 3. (a) Intervalley rates for SiC1-4 through multiple sequences of Li deposition, shown in log-log scale to highlight the power-law behavior. (b) The inverse mobility versus change of charge carrier density induced by Li deposition for SiC3 and SiC4, which were annealed to 700 and 900 K prior to cryogenic Li deposition. The dashed and solid lines in Figs. 3(a) and 3(b) show theoretical predictions based on the Dirac model (DM) and a tight-binding (TB) description, respectively.

conventional phase decoherence rate known from WL studies in metals. τ_i^{-1} and τ_*^{-1} are the intervalley and intravalley scattering rates corresponding to scattering between or within a single valley, respectively [Fig. 1(a)]. τ_*^{-1} is very high in epitaxial graphene, even without Li, due to chirality-breaking disorder and trigonal warping [26–28]. As a result, the last term in Eq. (1) is suppressed and not included in our fits.

Extracted values of τ_φ^{-1} were nearly independent of Li coverage, even over an order of magnitude increase in carrier density [Fig. 2(b)]. This can be understood from the fact that Li is a light adatom, and not a source of spin-orbit coupling or magnetism [7]. The contribution to the dephasing rate due to electron-electron interactions would be expected to rise from 11 to 26 ns^{-1} for the data in Fig. 2, as conductivity decreased from 134 to $42e^2/h$ with added Li [Fig. 1(c)] [25,28]. However, this represents a small perturbation on the overall dephasing rate, which, in epitaxial graphene on SiC, is dominated by magnetic impurities [29,30].

In contrast, τ_i^{-1} increased significantly after Li deposition [Fig. 2(c)], ultimately to values so high that the second term in Eq. (1) was suppressed and the error bars in the extracted τ_i^{-1} extend off the top of the graph (see Ref. [25] for details on fitting). These half error bars indicate that the extracted τ_i was indistinguishable from zero within experimental uncertainty, which was limited primarily by the 100 mT scan range of the coil.

Figure 3(a) compiles τ_i^{-1} for six samples, presenting a series of Li depositions for each sample. It confirms the consistently strong increase of intervalley scattering as Li is added, in spite of the common expectation that alkali-metal adatoms should have minimal effect on intervalley scattering [9,13,31]. A clue to understanding this surprising result comes from the functional form of the scattering rate increase, seen clearly in the log-log plot of Fig. 3(a): the measured τ_i^{-1} fits well to a $\tau_i^{-1} \propto \sqrt{n}$ dependence (dashed lines) up to a carrier density around 5×10^{13} cm^{-2}. Scattering rates for a given density of short-range scatterers would generically be proportional to the graphene density of states, which is $D(E_F) = 2\sqrt{n}/(\sqrt{\pi}\hbar v_F)$ within the linear Dirac model for graphene's band structure ($E = \hbar v_F k$). Thus, a $\sqrt{n}$ dependence is expected purely due to the doping effect from Li, enhancing the scattering rate from preexisting short-range defects in graphene on SiC [32] via the graphene density of states.

With τ_i^{-1} extracted from WL, τ_*^{-1} can then be determined from mobility as described in the Supplemental Material, Eq. (S21) [25]. Figure 3(b) illustrates the inverse mobility, $\mu^{-1} = en/\sigma$, for the two samples with highest carrier density. The close-to-linear relationship between μ^{-1} and Δn can also be explained within the Dirac model. In our experiment, the change in graphene carrier density, Δn, is proportional to the density of Li adatoms, n_{Li}. When conductivity is limited by Coulomb scattering off charged Li [9,12,13], one expects $\sigma \sim n/n_{\mathrm{Li}}$ giving $\mu^{-1} = (\sigma/en)^{-1} \sim \Delta n$.

The discussion above demonstrates that the modifications to intra- and intervalley scattering rates for low levels of Li doping can be approximately explained by the linear Dirac

model (DM). Above 5×10^{13} cm^{-2}, however, the intervalley data in Fig. 3(a) lies well above the $\sqrt{n}$ traces on the graph, indicating either (i) new short-range scatterers being added or activated, and/or (ii) deviations from the linear Dirac-cone density of states. The fact that the divergence between intervalley data and calculations only appears at high doping levels, and that Li adatoms or clusters would not be expected to bond strongly enough with the graphene to act as short-range scatterers [10,11,33,34], indicates that option (i) is unlikely.

In order to evaluate the second option, we perform numerical calculations of the scattering rate and conductivity/mobility based on the nearest-neighbor tight-binding (TB) description of the graphene bands. The TB description accounts for trigonal warping of the Dirac cones, illustrated by the constant energy contours in Fig. 1(a), as well as nonlinear corrections to the Dirac model. These corrections are important at the high carrier densities accessed in this work, where Fermi energies in excess of 1 eV are achieved (for a detailed discussion of DM and TB models, see Ref. [25]).

Our TB analysis is compared with experimental data through a calculation of scattering rates due to randomly distributed short-range defects and Li adatoms:

$$\tau_\alpha^{-1}(\varepsilon_{\mathbf{k}}) = \frac{2\pi}{\hbar} n_\alpha \int \frac{d\mathbf{k}'}{(2\pi)^2} \left|V^\alpha_{\mathbf{k}\mathbf{k}'}\right|^2 \delta(\varepsilon_{\mathbf{k}} - \varepsilon_{\mathbf{k}'}), \qquad (2)$$

where the index $\alpha = \{\text{Li, res}\}$ represents the disorder type, identifying whether the scattering originates from Li adatoms or from residual disorder, n_α is the areal density of the respective disorder, $\varepsilon_{\mathbf{k}}$ is the TB band energy, and $V^\alpha_{\mathbf{k}\mathbf{k}'}$ is the impurity matrix element for scattering from $\mathbf{k}$ to $\mathbf{k}'$ [25].

Coulomb scattering by the Li adatoms is described by a matrix element $V^{\text{Li}}_{\mathbf{k}\mathbf{k}'} \propto V_C(q, d)$ that is proportional to the 2D Fourier transform of the screened Coulomb potential, $V_C(q, d) = \frac{Z_{\text{Li}} e^2}{2\epsilon_0 \kappa \varepsilon(q)} \frac{e^{-qd}}{q}$. Here $q = |\mathbf{k} - \mathbf{k}'|$ is the scattering vector, $\kappa = (\varepsilon_{\text{SiC}} + 1)/2$ is the dielectric constant of the environment, $\varepsilon(q)$ is the static dielectric function of graphene, $Z_{\text{Li}} = 0.9$ is the expected valence of Li adatoms [10,11,17], and $d = 1.78$ Å is the expected distance between the Li adatoms and the graphene plane [17,35,36].

We assume that residual short-range disorder is dominated by atomic defects for which the scattering matrix element is momentum independent, therefore $V^{\text{res}}_{\mathbf{k}\mathbf{k}'} = V_{\text{res}}$, with different disorder strengths for intra- and intervalley scattering. Since V_{res} is explicitly not dependent on subsequent Li deposition, its value was extracted from the initial data for each sample (see Supplemental Material Table I [25]), leaving us with no free fitting parameters in our theory. TB and DM modeling were calculated using n_α's and V's for the residual short-range intra- and intervalley scattering extracted from the $\Delta n = 0$ values of μ, and τ_i in Fig. 3 (values of σ in Fig. 1 can be used instead of μ).

At low carrier densities where the DM applies, Eq. (2) yields a scattering rate that scales as $\tau_{\text{res}}^{-1} = \frac{n_{\text{res}} V_0^2 E_F}{\hbar^3 v_F^2} \propto \sqrt{n}$ as expected, consistent with the dependence of τ_i^{-1} below 5×10^{13} cm^{-2} in Fig. 3(a). The DM predictions (dashed lines) lie almost on top of the TB analysis (solid curves) at low density, confirming that the explanation of residual scatterers made more effective at higher carrier density survives the more accurate TB analysis.

At higher densities, the TB intervalley rates begin to deviate from the DM result due to the nonlinearity of the bands at high energies, but the effect is not nearly strong enough to account for the observed enhancement of the intervalley rate in the data. Therefore, even the second option discussed above (deviations from the linear Dirac-cone density of states) cannot explain the data within a noninteracting TB analysis. This experimental result is, however, consistent with recent ARPES studies [14–16] and theory [17], which indicate that the Dirac cone in alkali-doped graphene is strongly perturbed at high adatom densities. It is worth noting that the match between TB modeling and experimental data is much better in the carrier mobility [Fig. 3(b)], despite the lack of free fitting parameters. This can be attributed to the fact that the conductivity is limited by intravalley Coulomb-disorder scattering, while it is only weakly dependent on residual short-range scattering. It should thus be noted that it is our combined measurement of the zero-field conductivity and WL that has permitted a detailed analysis of the individual intra- and intervalley scattering rates, and it is this analysis that confirmed the discrepancy between experimental data and TB calculations of the scattering rates.

In summary, Li adatoms deposited in cryogenic UHV are observed to enhance both intervalley and intravalley carrier scattering rates in epitaxial graphene. The enhancement of the intravalley rates is quantitatively explained by Coulomb scattering off the ionized Li dopants that remain on the graphene surface, based on a calculation with no free fitting parameters. The enhancement of the intervalley rate, while surprising for an alkali-metal atom like Li that bonds weakly to graphene and causes minimal short-range scattering, can largely be explained by enhanced scattering off preexisting short-range scatters.

At the highest carrier densities observed in this work, however, deviations between our TB calculations and the experimental data do appear. This may originate from effects not accounted for by our TB model, such as the above-mentioned modifications of the graphene bands observed in ARPES and theory [14–17]. Other possible explanations could be as follows: Our TB model may use an incorrect position of the van Hove singularity in the graphene density of states, which is predicted by density functional theory to lie at a much lower energy [17]. Resonant scattering [37–39] off the Li impurity band [14,17] may play a role, as the impurity band associated with Na ions was shown to modify the transport properties of Si metal-oxide-semiconductor field-effect transistors significantly [40,41], but theoretical predictions for the contribution of this mechanism to intervalley scattering are too weak to explain the experimental data [17]. Nonlocal screening may enhance intervalley scattering by charged impurities [42]. Or, the Dirac cones themselves may be modified by electron-electron interactions [43].

The data reported here present a comprehensive picture of intervalley and intravalley scattering in adatom-doped graphene. We hope that they will help in relating ARPES and transport experiments that have until now offered disconnected pictures of scattering rates in, respectively, high and low density regimes [9,12–16,44]. Inconsistencies uncovered

in this work point to the need for further experimental and theoretical investigation of the electronic structure and scattering mechanisms in graphene, in order to fully unravel the properties of graphene with alkali-metal adatoms.

The authors acknowledge D. Bonn, S. Burke, A. Damascelli, G. Levy, B. Ludbrook, A. Macdonald, P. Nigge, A. Pályi, and E. Sajadi for numerous discussions, as well as B. Ludbrook and J. Renard for assistance in building the chamber. K.K. acknowledges support from the European Union's Horizon 2020 research and innovation programme under the Marie Sklodowska-Curie Grant Agreement No. 713683 (COFUNDfellowsDTU). The Center for Nanostructured Graphene (CNG) is sponsored by the Danish National Research Foundation, Project DNRF103. A.K. thanks UBC for financial support through the Four Year Doctoral Fellowship. Research supported by NSERC, CFI, and the SBQMI in partnership with MPI.

[1] G. Profeta, M. Calandra, and F. Mauri, Nat. Phys. **8**, 131 (2012).
[2] J. A. Flores-Livas and A. Sanna, Phys. Rev. B **91**, 054508 (2015).
[3] B. Uchoa and A. H. Castro Neto, Phys. Rev. Lett. **98**, 146801 (2007).
[4] R. Nandkishore, L. S. Levitov, and A. V. Chubukov, Nat. Phys. **8**, 158 (2012).
[5] X. Hong, K. Zou, B. Wang, S.-H. Cheng, and J. Zhu, Phys. Rev. Lett. **108**, 226602 (2012).
[6] T. Eelbo, M. Waśniowska, P. Thakur, M. Gyamfi, B. Sachs, T. O. Wehling, S. Forti, U. Starke, C. Tieg, A. I. Lichtenstein, and R. Wiesendanger, Phys. Rev. Lett. **110**, 136804 (2013).
[7] C. Weeks, J. Hu, J. Alicea, M. Franz, and R. Wu, Phys. Rev. X **1**, 021001 (2011).
[8] J. Hu, J. Alicea, R. Wu, and M. Franz, Phys. Rev. Lett. **109**, 266801 (2012).
[9] J.-H. Chen, C. Jang, S. Adam, M. S. Fuhrer, E. D. Williams, and M. Ishigami, Nat. Phys. **4**, 377 (2008).
[10] K. T. Chan, J. B. Neaton, and M. L. Cohen, Phys. Rev. B **77**, 235430 (2008).
[11] X. Liu, C. Z. Wang, Y. X. Yao, W. C. Lu, M. Hupalo, M. C. Tringides, and K. M. Ho, Phys. Rev. B **83**, 235411 (2011).
[12] J. Katoch and M. Ishigami, Solid State Commun. **152**, 60 (2012).
[13] J. Yan and M. S. Fuhrer, Phys. Rev. Lett. **107**, 206601 (2011).
[14] B. M. Ludbrook, G. Levy, P. Nigge, M. Zonno, M. Schneider, D. J. Dvorak, C. N. Veenstra, S. Zhdanovich, D. Wong, P. Dosanjh, C. Straßer, A. Stöhr, S. Forti, C. R. Ast, U. Starke, and A. Damascelli, Proc. Natl. Acad. Sci. USA **112**, 11795 (2015).
[15] J. L. McChesney, A. Bostwick, T. Ohta, T. Seyller, K. Horn, J. González, and E. Rotenberg, Phys. Rev. Lett. **104**, 136803 (2010).
[16] A. V. Fedorov, N. I. Verbitskiy, D. Haberer, C. Struzzi, L. Petaccia, D. Usachov, O. Y. Vilkov, D. V. Vyalikh, J. Fink, M. Knupfer, B. Büchner, and A. Grüneis, Nat. Commun. **5**, 3257 (2014).
[17] K. Kaasbjerg and A.-P. Jauho, arXiv:1904.08191 .
[18] M. Kühne, F. Paolucci, J. Popovic, P. M. Ostrovsky, J. Maier, and J. H. Smet, Nat. Nanotechnol. **12**, 895 (2017).
[19] C. Straßer, B. M. Ludbrook, G. Levy, A. J. Macdonald, S. A. Burke, T. O. Wehling, K. Kern, A. Damascelli, and C. R. Ast, Nano Lett. **15**, 2825 (2015).
[20] J. Li, L. Lin, D. Rui, Q. Li, J. Zhang, N. Kang, Y. Zhang, H. Peng, Z. Liu, and H. Q. Xu, ACS Nano **11**, 4641 (2017).
[21] S. Wellnhofer, A. Stabile, D. Kochan, M. Gmitra, Y.-W. Chuang, J. Zhu, and J. Fabian, Phys. Rev. B **100**, 035421 (2019).
[22] S. Forti, K. V. Emtsev, C. Coletti, A. A. Zakharov, C. Riedl, and U. Starke, Phys. Rev. B **84**, 125449 (2011).
[23] Graphensic company, Epitaxial graphene on silicon carbide, http://graphensic.com.
[24] A. Khademi, E. Sajadi, P. Dosanjh, D. A. Bonn, J. A. Folk, A. Stöhr, U. Starke, and S. Forti, Phys. Rev. B **94**, 201405 (2016).
[25] See Supplemental Material at http://link.aps.org/supplemental/10.1103/PhysRevB.100.161405 for photographs of several samples on the stage, conductivity data for other samples, calculated contribution to the dephasing rate from electron-electron interactions, weak localization curves' fitting procedure, theoretical tight-binding and Dirac modeling, and discussion about lack of superconductivity in Li-doped graphene.
[26] E. McCann, K. Kechedzhi, V. I. Fal'ko, H. Suzuura, T. Ando, and B. L. Altshuler, Phys. Rev. Lett. **97**, 146805 (2006).
[27] Y.-F. Chen, M.-H. Bae, C. Chialvo, T. Dirks, A. Bezryadin, and N. Mason, J. Phys.: Condens. Matter **22**, 205301 (2010).
[28] F. V. Tikhonenko, D. W. Horsell, R. V. Gorbachev, and A. K. Savchenko, Phys. Rev. Lett. **100**, 056802 (2008).
[29] S. Lara-Avila, S. Kubatkin, O. Kashuba, J. A. Folk, S. Lüscher, R. Yakimova, T. J. B. M. Janssen, A. Tzalenchuk, and V. Fal'ko, Phys. Rev. Lett. **115**, 106602 (2015).
[30] S. Lara-Avila, A. Tzalenchuk, S. Kubatkin, R. Yakimova, T. J. B. M. Janssen, K. Cedergren, T. Bergsten, and V. Fal'ko, Phys. Rev. Lett. **107**, 166602 (2011).
[31] B. Yan, Q. Han, Z. Jia, J. Niu, T. Cai, D. Yu, and X. Wu, Phys. Rev. B **93**, 041407 (2016).
[32] P. Mallet, I. Brihuega, S. Bose, M. M. Ugeda, J. M. Gómez-Rodríguez, K. Kern, and J. Y. Veuillen, Phys. Rev. B **86**, 045444 (2012).
[33] X. Fan, W. T. Zheng, J.-L. Kuo, and D. J. Singh, ACS Appl. Mater. Interfaces **5**, 7793 (2013).
[34] M. Liu, A. Kutana, Y. Liu, and B. I. Yakobson, J. Phys. Chem. Lett. **5**, 1225 (2014).
[35] F. Valencia, A. H. Romero, F. Ancilotto, and P. L. Silvestrelli, J. Phys. Chem. B **110**, 14832 (2006).
[36] M. Farjam and H. Rafii-Tabar, Phys. Rev. B **79**, 045417 (2009).
[37] T. O. Wehling, M. I. Katsnelson, and A. I. Lichtenstein, Phys. Rev. B **80**, 085428 (2009).
[38] T. O. Wehling, S. Yuan, A. I. Lichtenstein, A. K. Geim, and M. I. Katsnelson, Phys. Rev. Lett. **105**, 056802 (2010).
[39] S. Irmer, D. Kochan, J. Lee, and J. Fabian, Phys. Rev. B **97**, 075417 (2018).
[40] A. B. Fowler and A. Hartstein, Philos. Mag. B **42**, 949 (1980).
[41] T. Ando, A. B. Fowler, and F. Stern, Rev. Mod. Phys. **54**, 437 (1982).
[42] P. Boross and A. Pályi, Phys. Rev. B **92**, 035420 (2015).
[43] T. Stauber, P. Parida, M. Trushin, M. V. Ulybyshev, D. L. Boyda, and J. Schliemann, Phys. Rev. Lett. **118**, 266801 (2017).
[44] U. Chandni, E. A. Henriksen, and J. P. Eisenstein, Phys. Rev. B **91**, 245402 (2015).